Research Square

Preprints are preliminary reports that have not undergone peer review.
They should not be considered conclusive, used to inform clinical practice,
or referenced by the media as validated information.

Interaction of L-Tryptophan in Aqueous Solutions with Platinum and Gold Nanoparticles of Different Morphologies

Galina Kupriyanova
Immanuel Kant Baltic Federal University
Mark Smirnov
smirnov.mark2015@yandex.ru

Immanuel Kant Baltic Federal University
Ivan Mershiev
Immanuel Kant Baltic Federal University
Aleksandr Zozulya
Immanuel Kant Baltic Federal University
Andrey Zyubin
Immanuel Kant Baltic Federal University

Research Article

Keywords:

Posted Date: May 20th, 2026

DOI: https://doi.org/10.21203/rs.3.rs-9644504/v1

License: This work is licensed under a Creative Commons Attribution 4.0 International License.
Read Full License

Additional Declarations: No competing interests reported.

Version of Record: A version of this preprint was published at Applied Magnetic Resonance on July 14th, 2026. See the published version at https://doi.org/10.1007/s00723-026-01849-5.

Abstract

This study presents for the first time a comprehensive study of the mechanisms of interaction L-tryptophan (L-Trp) in aqueous solution with platinum (Pt) and gold nanoparticles (Au NPs) of different shapes based on ^{1}H NMR, DOSY spectroscopy, T_1 relaxation measurements and data analysis. The paper introduces criteria for assessing the degree of L-Trp binding to Au NPs, including the probability of π -stacking, such as the multidirectional changes in chemical shift, the slowing of molecular motion, and the contribution of surface-induced relaxation. Based on these criteria, it is shown that the mechanism of interaction between L-Trp and Au NPs is critically dependent on Au NP morphology. The diffusion coefficient data set demonstrates that rod- and star-shaped Au NPs have a significantly stronger effect on translational diffusion than their spherical counterparts, reflecting differences in surface morphology, contact area, and heterogeneity of binding sites (L-Trp : $D = (6.62 \pm 0.05) \times 10^{-10}$ m²/s, L-Trp + Au RNP: $D = (5.49 \pm 0.17) \times 10^{-10}$ m²/s; L-Trp + Au SNP: $D = (5.90 \pm 0.10) \times 10^{-10}$ m²/s).

Introduction

In last years, there has been growing interest in translating advances in nanotechnology into medicine, particularly in the use of noble metal nanoparticles for the delivery of therapeutic agents as well as for diagnostic and therapeutic applications [1–4]. Gold nanoparticles (Au NPs) have been widely investigated owing to their low cytotoxicity and stability under varying conditions, including changes in temperature and pH [5]. These properties of Au NPs make them promising candidates for use as therapeutic agents and drug carriers [6–8]. Platinum nanoparticles (Pt NPs) are attracting increasing attention as potential anticancer agents due to their antitumor properties.

Recently developed techniques for the functionalization of NPs [1, 9] with bioorganic molecules have significantly reduced the particles' effects on living cells and enhanced biocompatibility, thereby facilitating the targeted delivery of therapeutic agents [6–8, 10]. As one of the natural amino acids with hydrophobic properties, tryptophan (Trp) is particularly promising for the functionalization of NPs and the enhancement of their biological activity [11]. A notable example of enhanced biological activity is the ability of tryptophan-functionalized Au NPs to inhibit insulin aggregation, a process free Trp molecules are incapable of preventing. Moreover, suppression of protein aggregation is defined by the conformational state of amino acids functionalized with Au NPs [12].

However, owing to the presence of the indole group, L-tryptophan (L-Trp) exhibits unique spectral properties—strong absorption in the UV range ($\lambda max \approx 280$ nm) and intense fluorescence ($\lambda em \approx 350$ nm). These features render L-Trp a useful molecular probe for investigating interactions with NPs via optical spectroscopy. An earlier study of L-tryptophan interactions with zinc oxide nanoparticles has revealed the formation of stable complexes [13]. Spectroscopic analysis suggests that the dominant interactions between L-Trp and the nanoparticle surface are van der Waals forces and hydrogen bonds involving the carboxyl and indole groups [13]. In addition, the synthesis of nanostructures based on L-

Trp-functionalized Au NPs demonstrates strong adsorption of Trp molecules on the surface via both indole and carboxyl groups [11].

Density functional theory (DFT) analysis has shown that the most energetically favorable binding configuration involves simultaneous interactions through both the indole ring and the carboxyl group. The stability of the complex is primarily maintained by π-interactions of the indole ring [11, 14, 15]. Overall, these results indicate that L-Trp serves as an excellent model system for research, although experimental verification of these theoretical findings is required.

Several other significant issues remain poorly understood. To prevent particle aggregation and sedimentation, stabilizing agents are commonly employed in the synthesis of Au NPs [1]. Stabilizing molecules adsorb onto the nanoparticle surface, forming an organic shell that can significantly modify the surface properties of the nanoparticles and affect the binding mechanism and dynamics of nanoparticles augmented with amino acids. Understanding the influence of stabilizing molecules on the interaction between amino acids and nanoparticles is an important but understudied aspect of nanoparticle biochemistry [1].

Another key issue that requires investigation is the extent to which particle morphology affects the mechanisms of amino acid binding and the dynamic characteristics of the system (AC-NP). Since rod- and star-shaped gold nanoparticles exhibit plasmon resonances distinct from those of spherical particles, nanoparticles of different shapes are likely to exhibit different binding properties toward amino acids. According to the literature [16], particle shape, as well as size and composition, influences cellular uptake. Correspondingly, analysis of the translational and rotational motion of an AS141 aptamer has revealed higher directional diffusion rates for AS1411 bound to gold stars compared with AS1411 bound to 50-nm spherical gold particles [16].

The role of NP morphology in binding mechanisms and dynamic behavior in the presence of Trp remains incompletely understood. An important method for elucidating the interaction mechanisms between nanoparticles and amino acids and for characterizing the dynamic behavior of the NP-AA system is NMR, which is also effective for identifying conformational changes in molecules near NPs. Relaxation NMR and NOESY methods have proven to be reliable and sensitive probes of dynamic motion across a wide temporal range, enabling the study of both picosecond-scale molecular vibrations and millisecond-scale conformational changes [17–19]. Trp has been employed like a probe to monitor conformational changes in proteins, using ^{1}H-^{15}N NMR chemical shift data of the indole ring [20]. The combined use of ^{1}H NMR and NOESY has enabled the identification of conformational changes in L-tyrosine in the presence of Au NPs, with alterations in the spatial orientation of the CH_2–NH_2–COOH chain relative to the aromatic ring shown to depend on the shape of the Au NPs [21, 22].

Mathematical modeling employing various water models is essential for understanding the dynamic behavior of amino acids in aqueous solutions. Molecular motion near Au NPs has been simulated for 20 amino acids, and the diffusion coefficients and hydrodynamic radii have been calculated [16, 23]. Analysis of diffusion coefficient data for various amino acids, calculated using 11 different water

models, has revealed substantial variation in values [24], whereas another study [25] has not reported experimental diffusion coefficients for tyrosine or Trp. Obtaining data on amino acid diffusion coefficients, particularly for Trp, and on the effects of Au NPs on Trp diffusion is crucial for predicting the efficiency of biochemical processes involving nanoparticle–biomolecule systems and transport phenomena. From this perspective, several questions remain unanswered regarding how the shape, size, and type of NPs, specifically gold composition and morphology, influence the translational diffusion, rotational correlation times, and local molecular mobility of Trp. From this perspective, several questions remain unanswered regarding the influence of NPs of different shapes, sizes, and types on the dynamic behavior of Trp, particularly how gold composition and morphology affect translational diffusion, rotational correlation times, and local molecular mobility.

This paper investigates the influence of Pt NPs and Au NPs of various morphologies on the structure and dynamic properties of L-Trp in aqueous solution using ^{1}H NMR relaxation spectroscopy and ^{1}H NMR diffusion-ordered spectroscopy (DOSY), with the aim of elucidating the mechanisms of L-Trp interaction with metal nanoparticles as determined by NP morphology—spherical, rod-shaped, or star-shaped Au NPs—and NP type (Pt or Au). The study also examines the effect of the stabilizer, cetyltrimethylammonium bromide (CTAB), on the molecular and translational mobility of L-Trp in the presence of Au NPs. The findings are expected to contribute to a deeper understanding of amino acid–NP interactions and facilitate the rational design of nanoparticles for biomedical applications and drug delivery systems.

Materials

Sample Preparation

The focus of the study was on aqueous solutions of the amino acid L-Trp in the presence of spherical Pt NPs and Au NPs of various geometries. Three types of Au NPs were employed—spherical (Au NP), star-shaped (Au SNP), and rod-shaped (Au RNP) [21]. The L-tryptophan concentration in all samples was maintained at 10^{-3} mol/L to remain below saturation, which could otherwise hinder the analysis of binding kinetics [25].

To prepare samples for NMR analysis, 120 µL of aqueous L-Trp solution was combined with 48 µL of nanoparticle suspension (either Pt NPs or Au NPs of specified morphology). To stabilize resonance conditions and provide an internal chemical shift reference, 60 µL of deuterated water (D_2O) was added along with DSS (2,2-dimethyl-2-silapentane-5-sulfonic acid, 25 mM) as an internal standard. A further 370 µL of Milli-Q water was introduced to achieve a final sample volume of approximately 598 µL. The final sample composition included L-tryptophan (10^{-3} M), nanoparticles at the specified concentration, 10% v/v D_2O, and DSS as the internal reference.

Control experiments were conducted with (1) L-Trp in water containing equivalent amounts of D_2O and DSS, or (2) L-Trp with stabilizing agents in the absence of nanoparticles. These experiments enabled the

assessment of stabilizer effects on molecular dynamics, a critical aspect that has been insufficiently addressed in previous studies [1].

Samples were prepared immediately before measurement to minimize potential time-dependent changes in nanoparticle aggregation or complex dissociation kinetics. All measurements were conducted at 25.0 ± 0.1°C to ensure temperature consistency across experiments, an essential parameter affecting molecular diffusion and relaxation rates.

Pt NPs were synthesized via the polyol method [22, 26], following established protocols. Spherical Au NPs were prepared using the Turkevich method [27], while rod- and star-shaped Au NPs were synthesized according to previously described seed-mediated growth procedures [21], allowing precise control over morphology. Nanoparticle characterization was performed using scanning electron microscopy (SEM) to confirm morphology and estimate size distributions. NP sizes were estimated at approximately 40 nm in mean diameter for spherical particles, with rod-shaped and star-shaped particles having analogous dimensions. We already presented AuNPs shapes in our previous paper [21].

Methods

Spectrophotometry

The electronic absorption spectra of L-Trp in the presence of Au NPs and Pt NPs were obtained using a Shimadzu 1800 dual-beam spectrophotometer. Recorded spectra are over the wavelength range of 200–700 nm with optical densities from 0 to 3 relative units. Temperature was maintained at 25.0 ± 0.1°C using external control. Standard quartz cuvettes have a 1 cm optical path length. Aqueous solutions containing either Au or Pt NPs were titrated with L-Trp dissolved in water at a concentration of 0.05 mol/L, with a titration step of 2 µL.

^{1}H NMR Spectroscopy

^{1}H NMR spectra of an aqueous solution of L-Trp at 25°C were recorded on an Agilent (Varian) 400 MHz spectrometer at a ^{1}H operating frequency of 399.853 MHz. The experiments used a 90° pulse of 9.4 µs with a 1 s recycle delay and an 18 s acquisition time. The spectral width was 16.1 ppm, and 512 scans were recorded. The Water_ES pulse sequence was applied to suppress the water signal. To assign L-Trp signals in the ^{1}H NMR spectrum, correlation experiments such as ^{1}H–^{1}H COSY and TOCSY were performed in advance. Spectra were processed using MestReNova software.

The inversion-recovery sequence was used to measure the T_1 longitudinal relaxation times. To suppress the intense water signal during the relaxation experiments, the Presaturation pulse sequence was applied. The delay between pulse sequences was 10 s, and the number of scans (NS) for the relaxation experiment reached 256.

Diffusion-ordered NMR (^{1}H NMR DOSY) experiments were performed using a Doneshot pulse sequence and the Presat method to suppress the intense water signal. DOSY spectra were acquired with the following parameters: relaxation delay of 1 s, diffusion time Δ of 50.0 ms, gradient pulse duration of 2.0 ms, and gradient recovery delay of 0.5 ms. The gradient was ramped using 15 increments.

Results and Discussion

1. Spectrophotometric Analysis

Spectrophotometric analysis was performed on aqueous solutions of L-Trp with Au and Pt NPs to clarify the degree of change in the photoelectron spectrum of L-Trp in the presence of noble metal nanoparticles. UV–Vis spectra of L-Trp with Pt and Au NPs showed no distinct spectral shifts, in contrast to the behavior observed with L-tyrosine [22]. Minor deviations from the Beer–Lambert law at elevated NP concentrations indicate weak noncovalent interactions, but provide no evidence of new chromophore formation (Fig. 1a, b).

2. ^{1}H NMR Chemical Shifts

^{1}H NMR spectra of aqueous L-Trp solutions, both pure and in the presence of Au and Pt NPs, were investigated. Figure 2 (a, b) shows the molecular structure of L-Trp and fragments of the aromatic region of its ^{1}H NMR spectra recorded with and without the NPs.

Analysis of the ^{1}H NMR spectra of L-Trp indicates that the presence of Pt NPs affects the chemical shifts of aromatic ring protons. Minor downfield changes in chemical shifts of $\Delta\delta = 0.03–0.04$ ppm were observed for the *d*, *c*, and *b* protons (Fig. 2). In contrast, a more substantial downfield shift was recorded for the CH_2 proton lines of the side chain ($\Delta\delta = 0.2$ ppm) and the *f* proton of the indole ring ($\Delta\delta =$ 0.07ppm).

The opposite effect is observed in the L-Trp spectra in the presence of Au NPs. Figure 2 shows that the effect of Au NPs on L-Trp proton chemical shifts depends largely on particle morphology. While spherical Au NPs have virtually no effect on chemical shifts, Au SNPs and Au RNPs induce a downfield shift of $\Delta\delta \approx +0.20–+0.24$ ppm for the side-chain CH_2 proton lines, whereas a slight upfield shift of $\Delta\delta \approx -0.03$ to -0.06 ppm is observed for the *a* and *d* aromatic protons in the presence of Au RNPs. Remarkably, the directions of chemical shift changes for aromatic proton signals and the CH_2 side-chain proton lines are opposite for Au RNPs and Pt NPs. In the presence of Au RNPs, the change in chemical shifts may be due to a redistribution of electron density, an increase in the charge fraction in the aromatic fragment, or decreased density near the *f*-proton of the indole ring and near the side-chain protons. This indicates different mechanisms for the interaction of NPs and Pt NPs with L-Trp, supporting a π-stacking interaction for Au RNPs (the indole ring oriented parallel to the nanoparticle surface), in contrast to the charge-transfer mechanism observed with Pt NPs.

3. ^{1}H NMR Relaxation Time (T_1)

To conduct a detailed analysis of the influence of NPs on L-Trp and to gain deeper insight into interactions between NPs and L-Trp, the longitudinal (T_1) relaxation times of all resolved proton signals were measured in aqueous L-Trp solutions and in the presence of Au NPs with different morphologies. Analysis showed that T_1 values of the aromatic ring protons of L-Trp (*a*–*c*) in aqueous solution range from 2.30 s to 2.80 s, with a longer longitudinal relaxation time observed for the *d* proton (T_1 = 3.66 ± 0.02 s). Upon addition of NPs, the relaxation times of all protons decrease, indicating enhanced relaxation due to interactions with the NP surface.

Figure 3 presents a two-dimensional map of T_1 values measured for each line of the L-Trp spectrum in three samples, both in the absence and presence of Au SNPs and rod-shaped Au RNPs. Quantitative changes are summarized in Table 1 as the ratio of longitudinal relaxation times (T_1) for L-Trp protons in aqueous solution to T_1 in the presence of Au NPs of different morphologies. The data reveal a morphology-dependent effect: spherical and star-shaped Au NPs induce only minor changes in T_1 for the *b* and *c* protons, whereas the largest changes occur for the *a* and *d* aromatic protons, as well as the g_1 and g_2 protons of the CH_2 group. In contrast, rod-shaped Au NPs cause the most pronounced reduction in T_1, particularly for the *a* and *d* aromatic protons and the aliphatic CH_2 protons.

Control experiments were conducted to assess the contribution of the stabilizer, CTAB, which was added to an aqueous solution of L-Trp without nanoparticles. Surprisingly, CTAB alone caused a significant decrease in the T_1 relaxation time—28–30% for the *a* proton and 68% for the *d* proton. This indicates the limited mobility of L-Trp, which may result from the formation of a unique shell, possibly micellar one, around the molecule. However, this effect is mitigated by the addition of Au NPs. When Au NPs are introduced into a system containing CTAB, the effect is partially reversed: T_1 values for the *b* and *c* protons increase relative to those in the presence of CTAB alone. This suggests that Au NPs compete with the formed shell for L-Trp binding, effectively “extracting” the amino acid from a viscous, possibly micellar, phase and placing it in a microenvironment where its molecular structure is sterically hindered. The presence of rod-shaped NPs is associated with a marked reduction in T_1 values for all protons compared with the CTAB-only system, confirming that the dominant relaxation enhancement results from direct interaction with the NP surface rather than with the stabilizer.

With the addition of Pt NPs, the longitudinal and transverse relaxation times tend to decrease for all protons, with a significantly stronger effect observed for the side-chain protons of L-Trp. Specifically, the T_1 relaxation times of the CH_2 protons (g_1, g_2) decrease by factors of 1.6 and 1.2, respectively, while the *h* proton of the side chain exhibits a 1.86-fold reduction. In contrast, aromatic protons exhibit only a modest (~ 3–5%) shortening of T_1.

Table 1
Ratio of T_1 longitudinal relaxation times of L-Trp protons in aqueous solution to proton T_1 relaxation times in the presence of NPs

Proton	T_1 (L-Trp)/ T_1 (L-Trp + Pt NPs)	T_1 (L-Trp)/ T_1 (L-Trp + Au NPs)	T_1 (L-Trp) / T_1 (L-Trp + Au SNPs)	T_1 (L-Trp) / T_1 (L-Trp + CTAB)	T_1 (L-Trp)/ T_1 (L-Trp + Au RNPs)
a	1.03	1.29	1.38	1.44	1.79
d	1.02	1.15	1.20	2.64	3.25
f	1.05	1.62	1.63	1.75	2.41
c	1.04	1.00	1.05	1.28	1.78
b	1.06	1.01	1.05	1.26	1.86
h	-	-	-	0.88	1.54
g	1.61	2.20	1.79	1.45	1.55
CH_2	1.22	1.69	1.67	1.346	-

4. Diffusion-Ordered Spectroscopy (DOSY)

^{1}H NMR diffusion-ordered spectroscopy (DOSY) experiments were performed to further investigate the interaction between L-Trp and Au NPs of different morphologies and to quantify translational diffusion coefficients. The experimentally measured diffusion coefficients are summarized in Table 2. In pure aqueous solution, L-Trp exhibits a diffusion coefficient of $D = (6.62 \pm 0.05) \times 10^{-10}$ m² s⁻¹, in excellent agreement with both agar-gel measurements ($D = 6.27 \times 10^{-10}$ m² s⁻¹) [28, 29] and theoretical predictions based on the Stokes–Einstein equation ($D = 6.81 \times 10^{-10}$ m² s⁻¹).

Adding Au NPs reduces the diffusion coefficient, with the most pronounced effect observed for rod-shaped Au NPs ($D = (5.49\pm0.20) \times 10^{-10}$ m² s⁻¹). It is worth noting that the introduction of both rod- and star-shaped Au NPs is accompanied by the addition of CTAB, a surfactant employed to stabilize colloidal dispersion. A control sample containing L-Trp and CTAB (without NPs) was prepared to isolate the effect of the stabilizer. Interestingly, CTAB alone suppresses molecular mobility to a greater extent than CTAB-stabilized NPs, consistent with micelle-induced confinement of L-Trp within surfactant aggregates. It should be noted that the diffusion coefficient of L-Trp in the presence of only the stabilizer has the lowest value, equal to $D = (5.36\pm0.05) \times 10^{-10}$ m² s⁻¹, whereas the diffusion coefficient in the presence of stabilized Au NPs is higher than this value. As shown in Table 2, molecular mobility is highly sensitive to both the presence of the stabilizing agent and the morphology of the Au NPs. DOSY experiments are particularly useful for distinguishing the translational diffusion of different molecules in solution. Figure 4 shows that the mobility of the stabilizer is markedly lower than that of L-Trp, with CTAB exhibiting a diffusion coefficient of $D = 1.2 \times 10^{-10}$ m² s⁻¹. Crucially, 2D DOSY spectra reveals different

diffusion regimes within the same sample, with certain resonance regions exhibiting diffusion coefficients distinct from others (Fig. 4).

The diffusion coefficient of the aromatic protons of L-Trp decreases markedly in the presence of rod-shaped Au NPs, and the range of values expands considerably (Fig. 4). The broadest diffusion coefficient ranges are observed for the *d*, *b*, and *c* protons, possibly suggesting different conditions for binding interactions between this region of the L-Trp indole ring and Au RNPs in the presence of CTAB. In contrast, star-shaped Au NPs induce multimodal diffusion behavior of indole protons. The doublet lines corresponding to the *a* and *d* protons exhibit diffusion coefficients of $D_1 = (5.94 \pm 0.05) \times 10^{-10}$ m² s⁻¹ and $D_2 = 5.76 \times 10^{-10}$ m² s⁻¹, respectively, with a difference of approximately 3%. Yet, this difference exceeds the measurement error of ~ 12 %. Furthermore, the signals on the 2D map are clearly separated (Fig. 4b): in the presence of star- and rod-shaped Au NPs, the diffusion coefficient associated with the indole ring proton signal at δ = 7.1 ppm (*f* proton) is lower than that of other aromatic protons, falling in the range of $(5.6 \div 5.7) \times 10^{-10}$ m² s⁻¹. Although modest in magnitude, this splitting provides direct evidence of heterogeneous binding environments at the NP interface, where different segments of the same molecule experience unequal degrees of hydrodynamic coupling to the NP surface. This observation underscores the critical role of nanoscale surface topography: unlike the relatively uniform cylindrical surface of rod-shaped NPs, the branched, high-curvature architecture of star-shaped Au NPs creates multiple chemically and geometrically distinct adsorption sites. Despite the specific binding mechanisms of Au RNPs and Au SNPs, this heterogeneity provides direct evidence of site-specific binding, in which the indole moiety is immobilized on the NP surface, most likely via π-stacking. This interpretation has been supported by molecular dynamics simulations [23].

The authors [23] conducted a molecular dynamics (MD) study of the adsorption of each of the 20 amino acids on Au NPs have been performed using the GROMACS 4.5.5 package with the TIP4P water model and the OPLS-AA force field. Simulations revealed that L-Trp adsorbs onto the Au NP surface with its aromatic (indole) ring oriented parallel to the metal surface, a characteristic feature of π-stacking. The calculated self-diffusion coefficient of adsorbed L-Trp was $D = 0.17 \times 10^{-10}$ m² s⁻¹, which is substantially lower than the experimental DOSY values obtained in the present study. This discrepancy is likely attributable to the fact that the simulations were conducted for very small Au NPs (3–6 nm in diameter), whereas the system investigated here employed nanoparticles of ~ 40 nm, resulting in significantly lower surface coverage and more rapid exchange between free and bound states. It should be emphasized that the outcomes of MD investigations are strongly dependent on the selected water model.

An extensive comparative study [24] has been performed to evaluate the Amber ff99SB-ILDN force field for simulating amino acid hydration and diffusion using three-site (SPC, SPC/E, SPC/Eb, and TIP3P), four-site (TIP4P, TIP4P-Ew, and TIP4P/2005), and five-site (TIP5P and TIP5P-Ew) water models. The L-Trp diffusion coefficients calculated using these models span a wide range, from 6.7×10^{-10} m² s⁻¹ (TIP3P-FB) to 17.3×10^{-10} m² s⁻¹ (SPC). The value of $D = 6.7 \times 10^{-10}$ m² s⁻¹ obtained using the TIP3P-FB model is in excellent agreement with the present findings, thereby supporting the validity of the proposed interpretation.

An important dynamic parameter governing NPs mobility is the hydrodynamic radius, which can be determined both from molecular dynamics simulations and from experimental techniques relying on diffusion coefficient data. To estimate the hydrodynamic radii, r_h. of the L-Trp molecule in pure aqueous solution and in the presence of Au NPs, the Stokes–Einstein relation was employed in the following form [30]:

$$D = \frac{k_B T}{6\pi\, r_h \eta_{\,0}} \quad (1),$$

where k_B is the Boltzmann constant, T is temperature, and η_0 is the viscosity of water (η_0 = 0.89 mN·s/m²). Table 2 summarizes the hydrodynamic radii, r_h. The value obtained here for aqueous L-Trp is smaller than the hydrodynamic radius r_h = 3.6 Å reported in an earlier work [24], where the effective radius of L-Trp was calculated as a population-weighted average of the radii of individual low-energy conformers identified using the LowModeMD module with the MMFF94x force field. In the present study, the hydrodynamic radius increased in the presence of Au NPs, and reached its maximum value upon addition of CTAB to an aqueous solution of L-Trp.

Finally, Nefedova et al. [31] have employed diffusion-ordered spectroscopy (DOSY) to investigate L-Trp interactions in a polyoxometalate (POM)-based model complex, $(HTRP)_3PW_{12}O_{40}\cdot 5H_2O$. Diffusion coefficients and hydrodynamic radii were extracted from high-field (14 T) DOSY NMR spectra of samples prepared from aqueous mixtures of TiO_2-I, L-Trp (10 mM), and DSS (25 mM) in H_2O, subsequently dissolved in DMSO-d_6. Under these conditions, the diffusion coefficient of pure L-Trp was determined to be (7.68 ± 0.06) × 10^{-10} m² s^{-1}, substantially higher than the value obtained in the present study. This discrepancy can be attributed to differences in experimental conditions, particularly the use of DMSO-d_6 (which has lower viscosity than water at 25°C) and dissimilar sample preparation protocols.

5. Modeling the relaxation process

To clarify the mechanisms of interaction between L-Trp and nanoparticles, we modeled the NMR relaxation processes of the proton system in an aqueous solution of L-Trp, as well as in the presence of Pt NPs and Au NPs. The T_1 NMR relaxation times were measured with decoupled of spin-spin interactions. When modeling the relaxation processes, we ignored polarization transfer processes in the spin system. Proton spins were considered as a system of decoupled spin magnetic moments. Two main relaxation mechanisms were considered: intramolecular dipole-dipole relaxation, which takes into account all dipole-bound protons, and intermolecular relaxation, which is determined by diffusion processes in an aqueous solution of L-Trp and interactions with the solvent and nanoparticles. Measured diffusion coefficients and proton relaxation time data were used as the basis for the modeling. The rate of proton relaxation in L-Trp was determined by the expression:

$$R_i = R_i^{d-d} + R_i^{trans} + R_i^{surface}$$

The rate of intramolecular dipole-dipole relaxation is given by the expression [32]:

$R_i^{d-d} = \frac{3}{10} D_i^{d-d} \left(\frac{\tau}{w^2 \tau^{\,2} + 1} + \frac{\tau}{4\, w^2 \tau^{\,2} + 1} \right)$.

Here

$D_i^{d-d} = \Sigma_j D_{ij}^2 = \left(\frac{\mu_0}{4\pi} \right)^2 \Sigma_j \frac{\gamma^4 h^2}{(2\pi)^2 r_{ij}^6}$ is constant characterizing the dipole-dipoleinteraction, μ_0 = $4\pi * 10^{-7} H/m$ $\gamma^H = 2\ \pi * 42.58\ * 10^6 \frac{rad}{T}$ is gyromagnetic ratio of the proton; *h* = 6.63 $* 10^{-34}$J s is Planck's constant, W is the frequency at which nuclei are recorded, in our case w = $2\ \pi\ * 4.0 * 10^8$ $\frac{rad}{s}$, τ is the correlation time of rotational molecular motion.

We assumed that the correlation times of the molecular motion of the aromatic ring and side chain protons (g_1 and g_2) may differ, so two correlation times, τ_{slow} and τ_{fast} were introduced.

Intermolecular contributions are due to diffusion processes and interactions with the solvent and nanoparticles [33, 34].

The relaxation rate due to diffusion processes is

$$R_{1trans} = \frac{2}{15} \left(\frac{\mu_0}{4\pi} \right)^2 \gamma^4 h^2 n d^{-3} \mathrm{J} \left(\omega_0 \right)$$

where J(ω) = $\frac{\tau_{trans}}{1 + \omega^2 \tau_{trans}^2}$ is spectral density, which corresponds to the exponential correlation function for diffusive motion; τ_{trans}= $\frac{d^2}{D}$ is characteristic correlation time of translational diffusion, D is the diffusion coefficient in an aqueous solution, the value of which is taken from the DOSY experiment; n is concentration of water protons (~ 6.7×10²⁸ m⁻³); d is distance of closest approach (about ~ 4.5 Å). The contribution to the relaxation rate due to interaction with NPs is given by the expression:

$$R_{1\,(surface)} = \frac{R_{0\,(surface)}}{(d + d_0)^6}$$

Here, d is the distance from the proton to the NP surface (Å). The distance from the proton to the NP surface is optimized du ring calculations in the range of 3–10 Å () and d_0 is the effective minimum approximation, or "contact" parameter, taking into account the size of the water molecule and the CTAB layer. It was chosen to be 3.0 Å.

$R_{0(surface)}$ is the optimized parameter, accounting for the interaction of spins with the paramagnetic center on the particle surface, as well as the interaction with the protons of the CTAB stabilizer. This parameter is optimized in the range of 0.2 to 1.5 c⁻¹. Optimization was performed using a differential evolution algorithm with 19 parameters for L-Trp in the presence of Pt NPs and with 21 parameters for L-Trp with Au NPs. All geometric parameters were constrained within physical limits: bond lengths ± 5%, angles ± 10°, proton shifts within ± 0.3–0.4 Å. Diffusion coefficients were fixed at experimental values (or estimated values if they were not measured). Optimization was performed using differential evolution

with logarithmic error weighting. Fit quality was assessed by the mean error percentage, with values <12% considered excellent.

Table 2
Diffusion coefficients, correlation times of molecular motion and structural parameters extracted from ^{1}H NMR relaxation data and DOSY experiments for an aqueous solution of L-Trp and L-Trp in the presence of Pt NPs and Au NPs of different shapes.

Parameters	***L-Trp***	***L-Trp + Pt NPs***	***L-Trp + Au NPs***	***L-Trp + Au SNPs***	***L-Trp + Au RNPs***
r(g1-g2),A	1.24 (0.79[35])	1.176	1.19	1.152	1.027
r(g2-CH),A	1.59 (1.48[35])	1.49	1.50	1.38	1.28
τ_{islow} (10^{-12})s	4	6.1	4.34	4.61	5.36
τ_{ifast} (10^{-12})s	2	2.38	2.13	2.26	2.27
R_h	3.71	4.30	4.09	4.16	4.54
$R_{surface}$,s^{-1}	-	3.12	1.9	1.46	3.49
D, ($10^{10}m^2/s$)	6.62±0.05	5.7(*)	6.0 (*)	5.9±0.12	5.49±0.20, 5.40(*)

(*)-model values.

During the simulation, the distances between protons in the side chain and between protons in the CH_2 group were refined. In addition, the optimal correlation time for molecular motion was determined. The parameters obtained during the simulation are presented in the table T. For comparison, the Table 2 (T2) also includes data on the L-Trp structure from the database [35]. The obtained model data and experimental chemical shift data provide the basis for a deeper understanding of the interaction mechanisms.

Considering that the addition of platinum particles leads to changes in the chemical shifts of the side-chain protons and minor changes in the aromatic protons (+ 0.4 ppm for the CH protons and 0.28 ppm and 0.25 ppm for the g_1 and g_2 protons of the CH2 group, respectively), this indicates a redistribution of electron density. Considering the conformational rearrangement of the side chain and the slowing of the dynamics, it can be derived that the primary interaction mechanism is electrostatic, associated with the attraction of the charge to the platinum nanoparticle through the -OH chain. This leads to direct contact between the side chain and the particle, while the aromatic ring is deflected.

Considering the redistribution of electron density observed in the presence of Au NPs, we hypothesized that the most likely mechanism of interaction between the NPs and the L-Trp is π-stacking. The probability of π-stacking was assessed using a set of criteria based on chemical shift changes (Δδ), time delay dynamics (k = $\tau_{i\ slow}$(L-Trp + NPs)/($\tau_{i\ slow}$(L-Trp)), surface contribution $\left(R_{1\ (surface)}\right)$, and aromatic proton relaxation time ΔT_1 decrease.

Analysis shows that the Trp molecule binds to Au NPs via the side chain and COO– (hydrophobic mechanism), and the orientation of the side chain relative to the NP depends on the NP shape. Furthermore, the aromatic protons of indole can additionally interact with the NP surface via the π-electron cloud. In the presence of rod-shaped NPs, a upfield change in the chemical shift of all aromatic protons (-0.03 to -0.06 ppm), a pronounced slowing of molecular dynamics (k = 1.34), and the largest contribution of surface-induced relaxation ($R_{1\ (surface)}$, = 3.49 s^{-1}) are observed. Based on these criteria, we believe that in the presence of rod-shaped NPs the probability of π-stacking is highest, whereas in the presence of spherical Au NPs this probability will be minimal (minor change in chemical shift, k = 1.08, $R_{1\ (surface)}$ = 1.9) (Table 2). Thus, it can be concluded that the probability of π--stacking depends on the shape of the NPs.

Conclusion

A comprehensive analysis of data obtained from ^{1}H NMR and ^{1}H DOSY studies of L-Trp—including chemical shifts, measured T_1 relaxation times, and diffusion coefficients—revealed fundamental differences in the interaction mechanisms between L-Trp and NPs of different types (Pt and Au) and morphologies (spherical, star-shaped, and rod-shaped).

Pt nanoparticles added to aqueous L-Trp interact primarily via partial charge transfer, as evidenced by downfield shifts of aromatic protons (Δδ = 0.03–0.04 ppm) and the *f* proton of the indole ring, as well as more pronounced shifts (Δδ = 0.20–0.28 ppm) for side-chain protons. Relaxation measurements showed a significant reduction in T_1 relaxation times, indicating both the effect of uncompensated charge and a moderate restriction of molecular mobility, without formation of long-lived complexes.

Conversely, Au NPs induce oppositely directed changes in the chemical shifts of indolering and side-chain protons, depending on the Au NP morphology. The simulation results demonstrate that the mechanism of interaction between L-Trp and Au NPs is critically dependent on NP morphology.

Although all L-Trp and Au NPs systems exhibit side-chain adsorption (COO^-/NH_2), π-stacking of the indole ring is significantly enhanced for anisotropic nanorods NPs compared to spheres or stars. This conclusion is supported by a change in the chemical shift of all aromatic protons toward upfield values (-0.03 to -0.06 ppm), a pronounced slowing of molecular dynamics (k = 1.34), a larger contribution of surface-induced relaxation ($R_{1\ (surface)}$ = 3.49 s^{-1}), and aromatic proton relaxation time ΔT_1 decrease. Using these criteria, we can conclude that the binding of L-Trp molecules to Au NPs occurs via π-

stacking of the indole ring is weaker in the system with star-shaped Au NPs, and even weaker in the presence of spherical Au NPs.

Furthermore, the diffusion coefficient dataset extracted from DOSY experiments, through signal decay analysis in pulsed magnetic field gradients, provides the most direct evidence of the interaction of Au NPs with L-Trp. Nanoparticle morphology plays a crucial role here: non-spherical gold nanoparticles (rod- and star-shaped) exert a significantly stronger effect on translational diffusion than their spherical counterparts, reflecting differences in surface morphology, contact area, and heterogeneity of binding sites (Au RNP: $D = (5.49 \pm 0.17) \times 10^{-10}$ m²/s, ~ 17% reduction; Au SNP: $D = (5.90 \pm 0.10) \times 10^{-10}$ m²/s, ~ 11% reduction). Remarkably, star-shaped NPs exhibit multimodal diffusion behavior for indole protons, clearly demonstrating the presence of multiple structurally distinct binding microenvironments. The general trend in the presence of NPs, including Pt NPs and Au NPs (spherical, rod-, and star-shaped), is an increase in the relaxation rate, reflecting both reduced molecular mobility, as evidenced by decreased diffusion coefficients, and direct NP–L-Trp interactions.

Importantly, stabilizing agents, such as CTAB, exert a substantial influence on L-Trp dynamics, with effects comparable to or exceeding those of the NPs themselves. This highlights the necessity of control experiments, underscoring that the organic “corona” formed by synthesis surfactants—rather than the NP core alone—can dominate observed dynamical changes.

Overall, these findings confirm that ^{1}H NMR spectroscopy is a powerful tool for probing nanoparticle-induced changes in individual molecular fragments. This capability is critical for the quantitative analysis of biomolecular interactions with nanomaterials. The distinct binding paradigms—electron transfer for Pt nanoparticles and π-stacking for Au nanoparticles—and their sensitivity to nanoscale geometry lay a foundation for the rational design of functional nanoparticles for biomedical applications, with the most effective outcomes achieved through the combined optimization of composition, morphology, and surface chemistry.

Declarations

Author Contribution

G.K. and M.S. wrote the main manuscript text. G. K. also served as supervisor while the investigation was conducted by M.S. Andrey Zyubin and Aleksandr Zozulya's role was to provide resources for the research. I.M. provided the software that was used to conduct the study. All authors reviewed the manuscript.

Acknowledgments

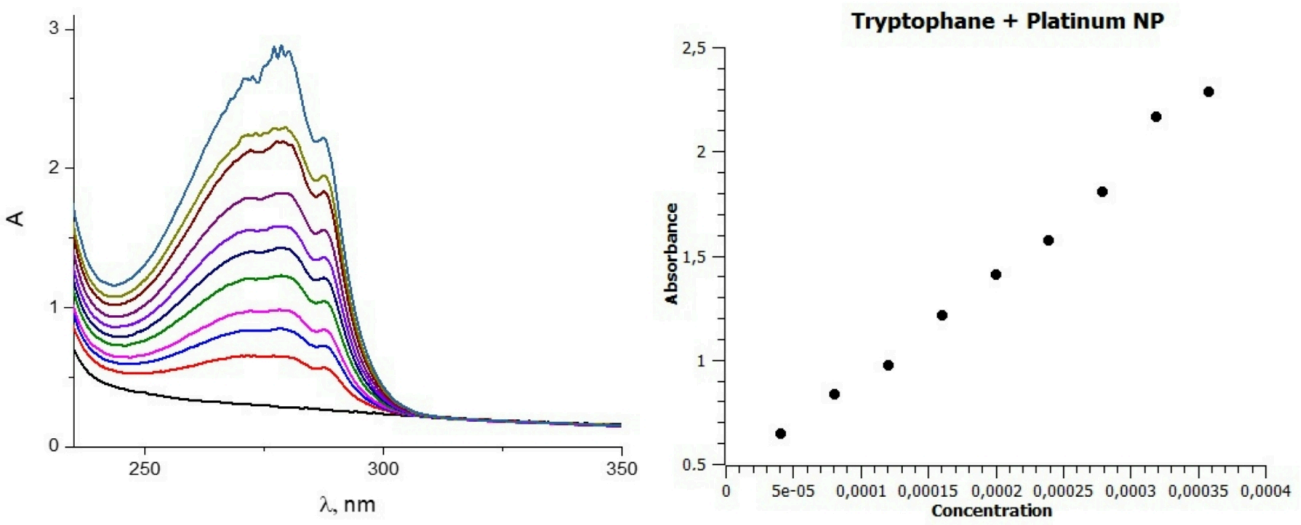
The research was carried out at the expense of the grant of the Russian Science Foundation No. 25-72-31032, https://rscf.ru/project/25-72-31032 /

References

1. G. Sanità, B. Carrese, A. Lamberti, Frontiers Mol. Biosci. (2020) https://doi.org/10.3389/fmolb.2020.587012;
2. T. Hassan, X. Huang, C. Zhou, M. Sikander, G. Khan, S. Saeed, Proc. Pakistan Acad. Sci. B Life Environ. Sci. (2021) https//doi.org/10.53560/PPASB;
3. E.O. Mikhailova, J. Funct. Biomater. (2021) https://doi.org/10.3390/jfb12040070;
4. J. Feng, R.B. Pandey, R.J. Berry, B.L. Farmer, R.R. Naik, H. Heinz, Soft Matter. (2011) https://doi.org/10.1039/C0SM01118E;
5. J. Georgeous, N. AlSawaftah, W.H. Abuwatfa, G.A. Husseini, Pharmaceutics. (2024) https://doi.org/10.3390/pharmaceutics16101332;
6. R.K. Delong, C.M. Reynolds, Y. Malcolm, A. Schaeffer, T. Severs, A. Wanekaya, Nanotechnol. Sci. Appl. (2010) https://doi.org/10.2147/NSA.S8984;
7. J.A. Zamora-Justo, P. Abrica-González, G.R. Vázquez-Martínez, A. Muñoz-Diosdado, J.A. Balderas-López, M. Ibáñez-Hernández, J. Nanomater. (2019) https://doi.org/10.1155/2019/5982047;
8. S. Akhtar, F. Zuhair, Int. J. Nanomedicine. (2025) https://doi.org/10.2147/IJN.S500978;
9. J.D. Pajović, R. Dojčilović, D.K. Božanić, S. Kaščáková, M. Réfrégiers, S. Dimitrijević-Branković, V.V. Vodnik, A.R. Milosavljević, E. Piscopiello, A.S. Luyt, V. Djoković, Colloids Surf. B Biointerfaces. (2015) https://doi.org/10.1016/j.colsurfb.2015.08.050;
10. V.S. Guido, P.H. Jr Olivieri, M.L. Brito, B.C. Prezoto, D.S.T. Martinez, M.L.V. Oliva, A.A. Sousa, Langmuir. (2024) https://doi.org/10.1021/acs.langmuir.4c01123;
11. A.I. Abd-Elhamid, H. El-Gendi, A.E. Abdallah, E.M. El-Fakharany, Pharmaceutics. (2021) https://doi.org/10.3390/pharmaceutics13101595;
12. K. Dubey, B. G. Anand, R. Badhwar, G. Bagler, P. N. Navya, H. K. Daima, K. Kar, Amino Acids. (2015) https://doi.org/10.1007/s00726-015-2046-6;
13. G. Mandal, S. Bhattacharya, T. Ganguly, Chem. Phys. Lett. (2009) https://doi.org/10.1016/j.cplett.2009.03.007;
14. P. Joshi, V. Shewale, R. Pandey, V. Shanker, S. Hussain, S.P. Karna, J. Phys. Chem. C. (2011) https://doi.org/10.1021/jp2070437;
15. J. Peng, L. Wang, P. Wang, Y. Pei, ACS Omega. (2023) https://doi.org/10.1021/acsomega.3c02195;
16. P. Choo, T. Liu, T. W Odom, J Am Chem Soc. (2021) https://doi.org/10.1021/jacs.1c00850;
17. R.P.R. Nanga, M.A. Elliott, A. Swain, N. Wilson, S. Swago, N.D. Soni, W.R. Witschey, R. Reddy, Magn. Reson. Med. (2022) https://doi.org/10.1002/mrm.29414;
18. I. Kuprov, L.C. Morris, J.N. Glushka, J.H. Prestegard, J. Magn. Reson. (2021) https://doi.org/10.1016/j.jmr.2020.106891;
19. A.C.F. de Albuquerque, F.M. Jr dos Santos, J. Braz. Chem. Soc. (2024) https://doi.org/10.21577/0103-5053.20230166;

20. M. T. Eddy, Zhan-Guo Gao, P. Mannes, N. Patel, K. A. Jacobson, V. Katritch, R. C. Stevens, K. Wüthrich, JACS. (2018) https://doi.org/10.1021/jacs.8b03805;
21. G. Kupriyanova, M. Smirnov, A. Zyubin, A. Zozulya, I. Lyatun, Appl. Magn. Reson. (2025) https://doi.org/10.1007/s00723-025-01781-0;
22. M. Smirnov, G. Gamov, A. Zyubin, A. Zozulya, I. Lyatun, E. Demishkevich, G. Kupriyanova, I. A. Khodov, J. Mol. Liq. (2025) https://doi.org/10.1016/j.molliq.2025.126822;
23. F. Ramezani, M. Amanlou, H. Rafii-Tabar, Amino Acids. (2014) https://doi.org/10.1007/s00726-013-1642-6;
24. H. Zhang, C. Yin, Y. Jiang, D. van der Spoel, J. Chem. Inf. Model. (2018) https://doi.org/10.1021/acs.jcim.8b00026;
25. A. Minj, S. Sahu, L. K. Singh Tanwar, K. K. Ghosh, RSC Adv. (2024) https://doi.org/10.1039/d4ra01872a;
26. E. E. Herricks, T. Thurnston, J. Chen, Y. Xia, Nano Lett. (2004) https://doi.org/10.1021/nl048570a;
27. J. Kimling, M. Maier, B. Okenve, V. Kotaidis, H. Ballot, A. Plech, J. Phys. Chem. B. (2006) https://doi.org/10.1021/jp061667w;
28. S. Miyamoto, K. Ekino, K. Shimono, Chem-Bio Inform. J. (2022) https://doi.org/10.1273/cbij.22.13;
29. S. Miyamoto, K. Atsuyama, K. Ekino, T. Shin, Chem. Pharm. Bull. (2018) https://doi.org/10.1248/cpb.c18-00071;
30. A. Einstein, Ann. Phys. (1905) https://doi.org/10.1002/andp.19053220806;
31. A. Nefedova, F. G. Svensson, A. S. Vanetsev, P. Agback, T. Agback, S. Gohil, L. Kloo, T. Tätte, A. Ivask, G. A. Seisenbaeva, V. G. Kessler, Inorg. Chem. (2024) https://doi.org/10.1021/acs.inorgchem.3c03674;
32. V.I. Chizhik, Y.S. Chernyshev, A. V. Donets, V. V. Frolov, A.V. Komolkin, M.G. Shelyapina, Magnetic Resonance and Its Applications, Springer Science & Business Media, Heidelberg (DE), 2014, pp. 1–785;
33. H.C. Torrey, Phys. Rev. (1953) https://doi.org/10.1103/PhysRev.92.962;
34. D.A. Faux, O. Istok, A.A. Rahaman, P.J. McDonald, E. McKiernan, D.F. Brougham, Phys. Rev. E. (2023) https://doi.org/10.1103/PhysRevE.107.054605;
35. https://pubchem.ncbi.nlm.nih.gov/compound/L-Tryptophan.

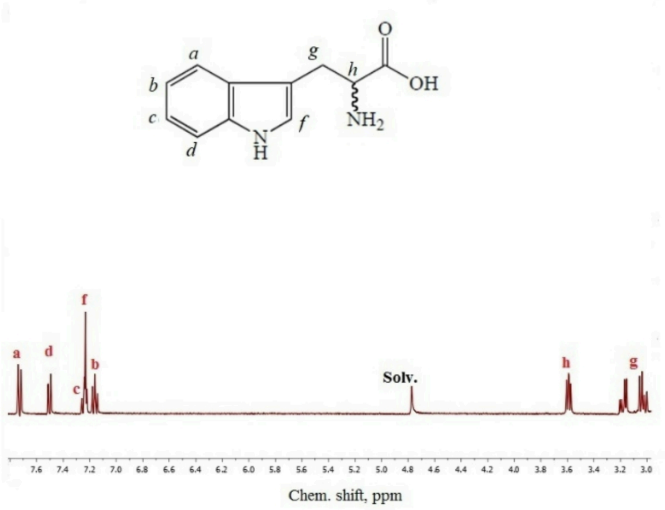
Figures



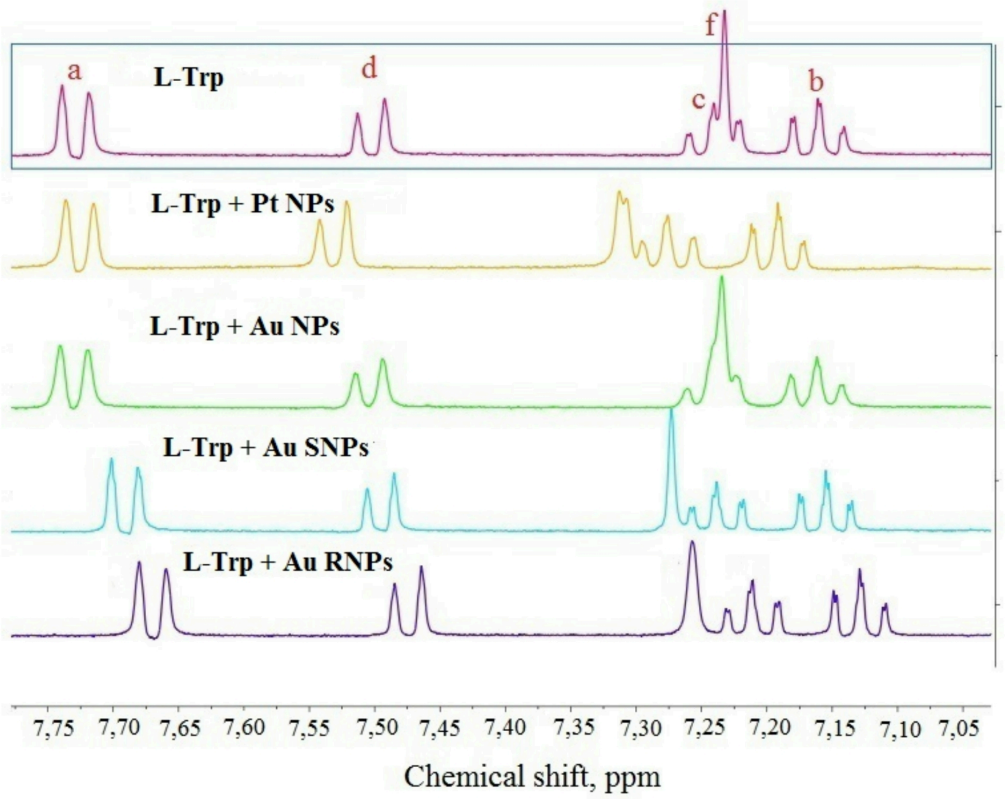
b)

Figure 1

(a) Electronic absorption spectrum of an aqueous L-Trp solution; (b) dependence of tryptophan absorbance on concentration in the presence of a platinum nanoparticle suspension at 279 nm



a)



b)

Figure 2

(a) ¹H NMR spectrum of L-Trp in aqueous solution; (b) fragment of the ¹H NMR spectrum showing the region of aromatic proton signals of an aqueous solution of L-tryptophan and L-tryptophan in the presence of Au and Pt NPs

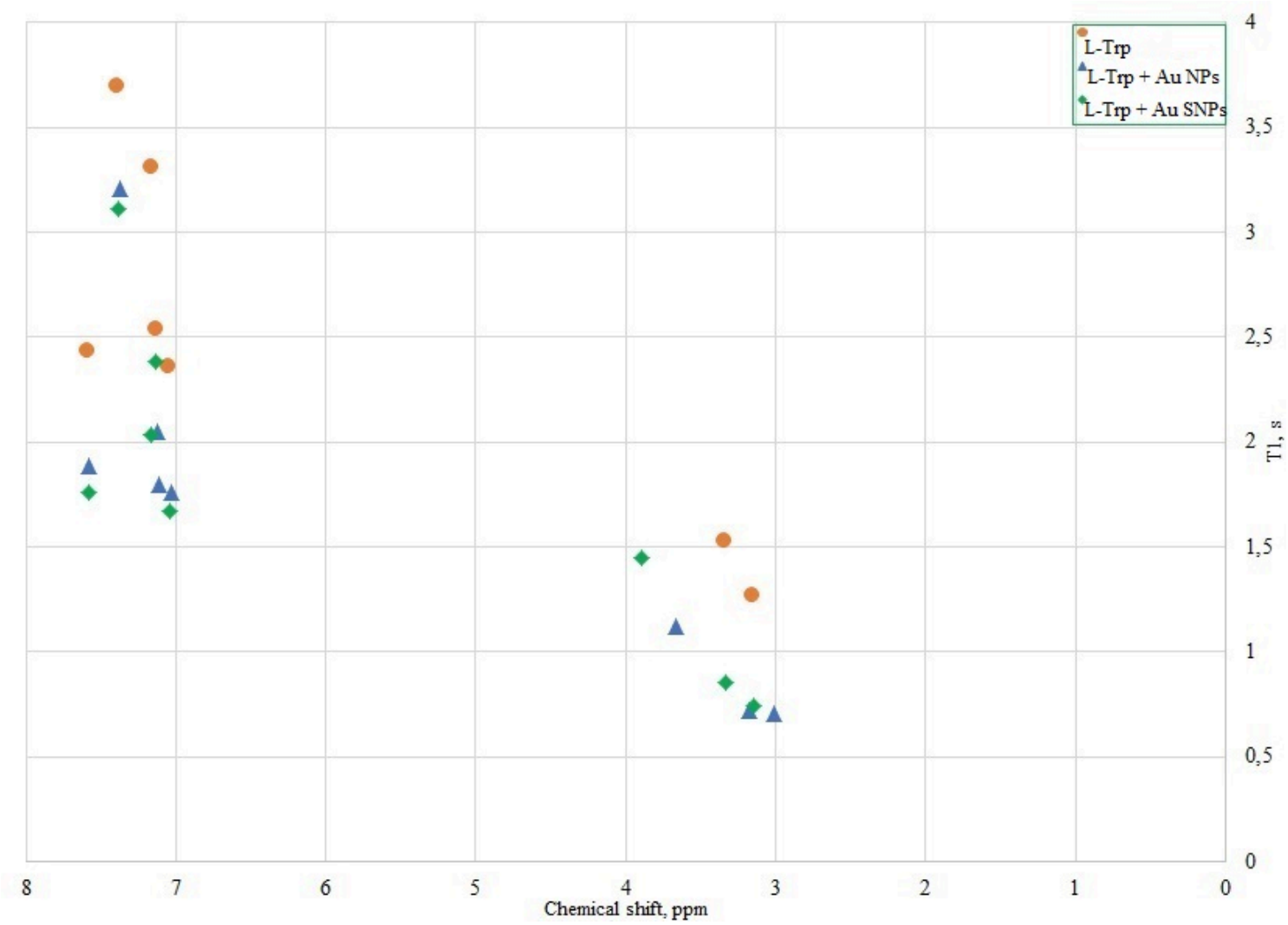
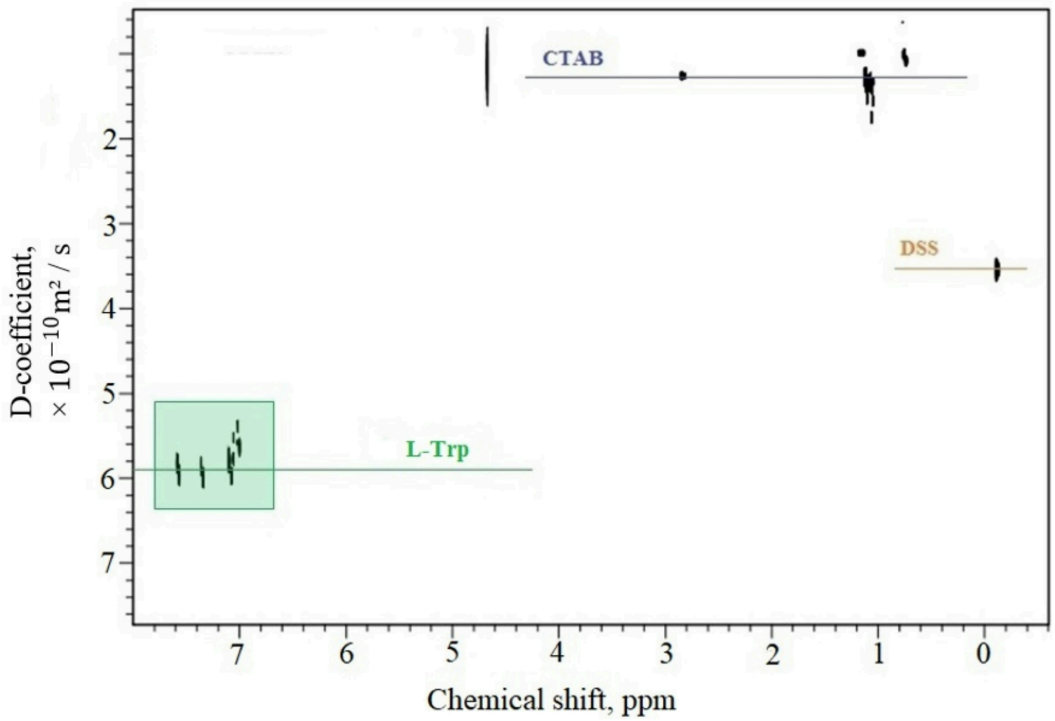
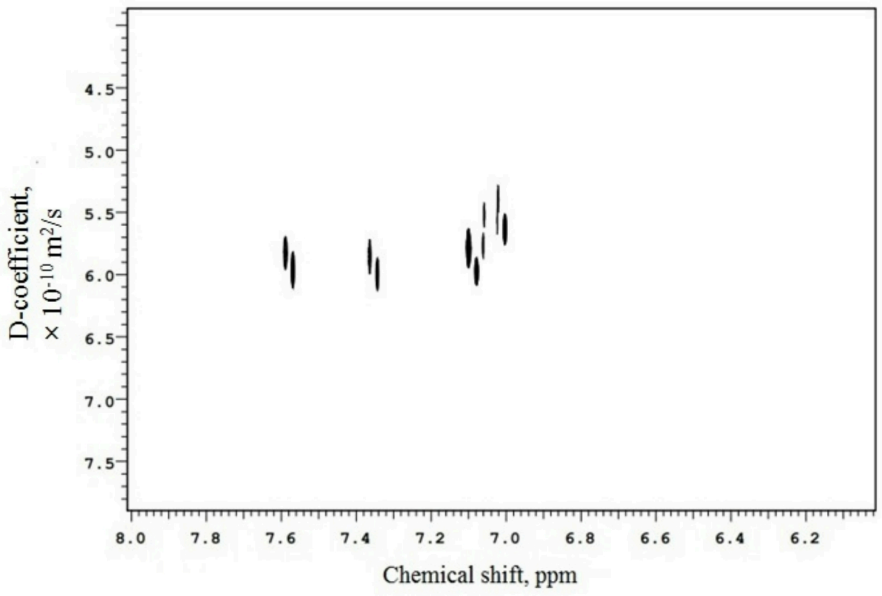


Figure 3

Two-dimensional map of longitudinal relaxation times (T_1) for protons of L-Trp in aqueous solution and in the presence of Au NPs of different morphologies



a)



b)

Figure 4

Diffusion-Ordered DOSY NMR spectrum of L-Trp in the presence of Au SNPs (a); aromatic region of the DOSY NMR spectrum of L-Trp in the presence of Au SNP (b)